

Stress pulse attenuation in shear thickening fluid

Weifeng Jiang, Xinglong Gong, Shouhu Xuan, Wanquan Jiang, Fang Ye et al.

Citation: *Appl. Phys. Lett.* **102**, 101901 (2013); doi: 10.1063/1.4795303

View online: <http://dx.doi.org/10.1063/1.4795303>

View Table of Contents: <http://apl.aip.org/resource/1/APPLAB/v102/i10>

Published by the [American Institute of Physics](#).

Related Articles

Frequency-modulated light scattering in colloidal suspensions
Appl. Phys. Lett. **102**, 061104 (2013)

Theory of nanoparticles doped in ferroelectric liquid crystals
J. Appl. Phys. **113**, 064308 (2013)

The effect of particle strength on the ballistic resistance of shear thickening fluids
Appl. Phys. Lett. **102**, 064103 (2013)

The internal structure of suspensions in uniaxial elongation
J. Appl. Phys. **113**, 044906 (2013)

Nanoparticle agglomeration in an evaporating levitated droplet for different acoustic amplitudes
J. Appl. Phys. **113**, 034307 (2013)

Additional information on *Appl. Phys. Lett.*

Journal Homepage: <http://apl.aip.org/>


Journal Information: http://apl.aip.org/about/about_the_journal

Top downloads: http://apl.aip.org/features/most_downloaded

Information for Authors: <http://apl.aip.org/authors>

ADVERTISEMENT

JANIS Does your research require low temperatures? Contact Janis today.
Our engineers will assist you in choosing the best system for your application.



10 mK to 800 K
Cryocoolers
Dilution Refrigerator Systems
Micro-manipulated Probe Stations

LHe/LN₂ Cryostats
Magnet Systems

sales@janis.com www.janis.com
Click to view our product web page.

Stress pulse attenuation in shear thickening fluid

Weifeng Jiang,¹ Xinglong Gong,^{1,a)} Shouhu Xuan,¹ Wanquan Jiang,² Fang Ye,² Xiaofeng Li,¹ and Taixiang Liu¹

¹CAS Key Laboratory of Mechanical Behavior and Design of Materials, Department of Modern Mechanics, University of Science and Technology of China (USTC), Hefei 230027, China

²Department of Chemistry, USTC, Hefei 230026, China

(Received 2 February 2013; accepted 28 February 2013; published online 11 March 2013)

The stress pulse attenuation of the 62 vol/vol. % dense silica particle-ethylene glycol suspension was investigated by using a modified split Hopkinson pressure bar. In comparison to the neat ethylene glycol solution, the transmission pulse of the shear thickening is much weaker under the same impact condition. No energy loss is progressed for the neat ethylene glycol solution, thus it can be concluded that the energy dissipation behavior was happened in the silica particle based shear thickening fluid. In this work, the energy dissipation of the shear thickening fluid was reversible. © 2013 American Institute of Physics. [<http://dx.doi.org/10.1063/1.4795303>]

Energy dissipation through a medium is an important subject and is crucial to a series of fields (e.g., earthquake protection and ballistic protection). It is generally acknowledged that the incident energy or stress wave attenuation under impact is due to the plastic (irreversible) failure. And the materials such as the metal foams are excellent energy absorbers owing to their deformation at a nearly constant stress level over a wide range of strain.^{1,2} However, it seems pretty clear that the energy dissipation processes for these materials are irreversible. Recently, granular materials were studied more extensively as a energy dissipation system. It was found that interparticle collision and friction mainly caused the energy dissipation, furthermore, the formation of the force chain was resulted in the impact load diffusion in space and time.^{3,4} Likewise, the grains would break when they suffered the strong impact load.

In this letter, we tested a dense suspension of colloidal particles. For this suspension, the particles are uniformly scattered in a carrier fluid. In this way, we do not need to worry about the particles damage, because each particle is under hydrostatic pressure condition which only changes the volume and does not produce plastic failure. In the last few decades, rheological experiments have been broadly carried out to investigate the effect of shear-thickening of such suspensions. Shear-thickening is a non-Newtonian behavior in which the effective viscosity increases with shear rate or shear stress, and recovers rapidly when the shear rate or shear stress is removed.⁵ This behavior has been linked to the formation of jamming particle clusters.⁶ Due to the highly non-Newtonian behavior, it is indicated that a shear thickening fluid (STF) is an excellent energy absorber, and it has been exploited in the damping⁷ and the body armor.^{8,9} In addition, a magnetorheological shear-thickening fluid (MRSTF) is worth noting. The shear-thickened structure is important for an MR fluid to obtain a high yield stress and prevent particle settling, which has contributed to some special applications.^{10,11} Here, this letter is to investigate the energy dissipation of the STF under dynamic impact. We found that the stress pulse energy decayed rapidly, when it

propagated through the STF. This behavior was reversible, and the deformation could be nearly neglected during the impact.

The STF based on silica particles (average diameter 400 nm) and ethylene glycol (density $\rho_{EG} = 1.11$ g/cc, bulk modulus $K_{EG} = 3.02$ GPa, sound velocity $c_{EG} = 1658$ m/s (Ref. 12)) with 62 vol/vol. % particle volume fraction are prepared. The energy change is tested on a modified split Hopkinson pressure bar (SHPB).¹³ In a standard SHPB set-up, a specimen is placed between two elastic bars (incident bar and transmission bar) and is loaded by a compressive pulse which resulted from the coaxial impact between the striker bar and the incident bar (see Fig. 1). The stress and strain conditions in the specimen during loading are evaluated by strain histories measured at the bars. In this case, the length of the pulse is much longer than the length of the specimen, and the stress pulse propagates through the specimen several times. In this letter, the classical SHPB set-up has been modified by extending the length of the specimen (about 100 mm) and shortening the length of the striker bar (30 mm). This arrangement allows that the single pulse characterization can be analyzed. The schematic of the modified SHPB is shown in Fig. 1. Both the incident bar and the transmission bar have length of 0.8 m. All bars are made of aluminum (elastic modulus $E_{AL} = 64.5$ GPa, sound velocity $c_{AL} = 5050$ m/s) with diameters of 14.5 mm. To confine and load the liquid specimen, the modified version of the SHPB has been completed with a cylindrical container and two pistons. The piston has a diameter of 14.5 mm and a length of 60 mm. They are also made of aluminum. The container is designed to limit the lateral deformation of the specimen and therefore is made of ordinary steel (elastic modulus $E_{ST} = 210.0$ GPa, sound velocity $c_{ST} = 5180$ m/s). It has an inner diameter of 14.6 mm, outer diameter of 25 mm, and a length of 160 mm. The container and the pistons fit together nicely and two gaskets are designed to avoid the spillage of the specimen (see Fig. 1). The diametrical clearance between the container and the piston is filled with Vaseline to reduce the container-pistons friction and avoid the spillage of the specimen. During the test: the striker bar which was fired out of a gas gun impacted the incident bar at the speed of

^{a)}Electronic address: gongxl@ustc.edu.cn.

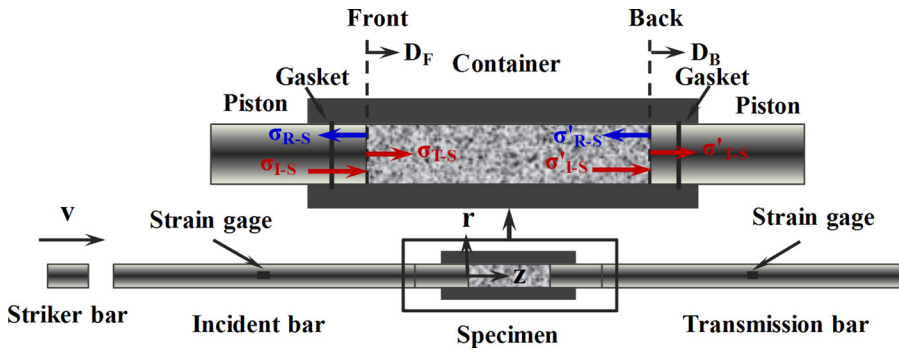


FIG. 1. The modified split Hopkinson pressure bar experimental schematic.

10–15 m/s, through which an incident pulse (σ_{I-S}) was generated and propagated through along the incident bar. As the incident pulse reached the front aluminum-specimen interface (see Fig. 1), a fraction of this pulse was reflected back (σ_{R-S}) and the rest was transmitted (σ_{T-S}) through the specimen. In the case of the pulse attenuation, the transmission pulse was reduced when the pulse reached the back of the specimen. The incident pulse, the reflection pulse, and the transmission pulse in the back specimen-aluminum interface were reported as σ'_{I-S} , σ'_{R-S} , and σ'_{T-S} , respectively. The single pulse attenuation was evaluated by comparing σ_{T-S} with σ'_{I-S} .

Because the specimen is confined by the hollow cylinder, the confining radial stress on the specimen is produced under the impact loading (Fig. 2(a)). So a part of the pulse energy is lost from the container. Thus, it is prohibitively difficult to evaluate the wave attenuation whether is caused by the specimen itself. Therefore, in this letter, the transmitted stress pulse of a system consisting of neat ethylene glycol is used as the reference pulse. It is proved that the energy dissipation of the ethylene glycol can be negligible besides the energy losing from the container. To this end, the theoretical incident pulse ($\bar{\sigma}'_{I-EG}$) of the back liquid-aluminum interface under this assumption and the measured incident pulse (σ'_{I-EG}) of the back liquid-aluminum interface are obtained and analyzed. The assumption is tenable, if the theoretical values coincide with the experimental values.

The stress analysis of the ethylene glycol is shown in Fig. 2(a), where z and r are the polar coordinates as defined in Fig. 1. The energy carried by a stress pulse can be obtained as

$$U_{P-S} = \frac{c_S A_S}{2K_S} \int_0^T \sigma_{P-S}^2(t) dt + \frac{\rho_S A_S c_S^3}{2K_S^2} \int_0^T \sigma_{P-S}^2(t) dt. \quad (1)$$

The first term is the strain energy and the second term is the kinetic energy, where c is the sound speed, A is the cross-sectional area, K is the elastic bulk modulus, ρ is the weight density, σ is the stress, T is the pulse length, and the subscript $P-S$ and S are the kind of stress pulse and the specimen, respectively. The sound speed c_S , the elastic bulk modulus K_S , and the weight density ρ_S are found to follow a relationship as shown,

$$\rho_S = \frac{K_S}{c_S^2}. \quad (2)$$

By inserting Eq. (2) into Eq. (1), it is clear that

$$U_{P-S} = \frac{c_S A_S}{K_S} \int_0^T \sigma_{P-S}^2(t) dt. \quad (3)$$

The energy conservation law which assuming that there is no energy loss by the ethylene glycol itself is used for analysis through which the energy conservation equation can be deduced,

$$\frac{c_{EG} A_{EG}}{K_{EG}} \int_0^T \sigma_{EG-z}^2(t) dt = \frac{4c_{ST} A_{EG} dz}{E_{ST} D_{EG}} \int_0^T \sigma_{EG-r}^2(t) dt + \frac{c_{EG} A_{EG}}{K_{EG}} \int_0^T [\sigma_{EG-z}^2(t) + 2\sigma_{EG-z}(t) d\sigma_{EG-z}(t)] dt, \quad (4)$$

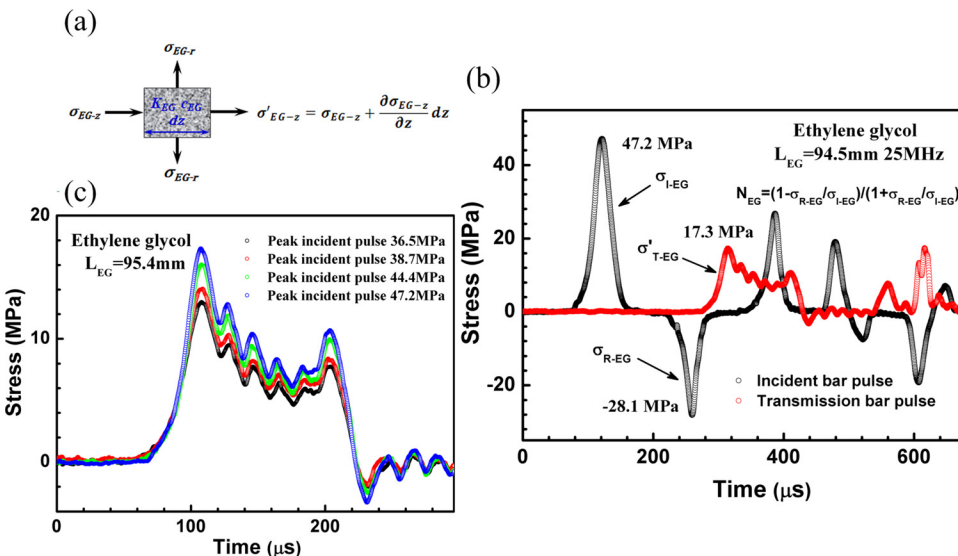


FIG. 2. (a) The stress analysis of the ethylene glycol; (b) The stress pulse of the ethylene glycol with a length of 95.4 mm under the peak incident stress 47.2 MPa; (c) The transmission pulse of ethylene glycol with a length 95.4 mm under the peak incident stresses of 36.5 MPa, 38.7 MPa, 44.4 MPa, and 47.2 MPa, respectively.

where σ_{EG-z} and σ_{EG-r} are axial stress and radial stress, respectively, the D_{EG} is the diameter of the ethylene glycol. It is considered that the axial stress equals to the radial stress.¹⁴ The left term is the input axial pulse energy, the first term in right is the radial pulse energy, the second term in right is the output axial pulse energy. The solution to Eq. (4) with the appropriate boundary condition ($z=0$, $\sigma_{EG-z}=\sigma_{T-EG}$) can be shown as

$$\sigma_{EG-z} = \sigma_{T-EG} e^{-\frac{2c_{ST}K_{EG}}{E_{ST}c_{EG}D_{EG}}z}. \quad (5)$$

The incident pulse (σ_{I-EG}), the reflection pulse (σ_{R-EG}) in the front end, and the transmission pulse (σ'_{T-EG}) in the back end can be measured by the strain gages (see Fig. 2(b)). According to these stress pulses, the acoustic impedance of the aluminum-liquid (N_{EG}) and the liquid-aluminum (N'_{EG}) are calculated from

$$N_{EG} = \frac{1 - \frac{\sigma_{R-EG}}{\sigma_{I-EG}}}{1 + \frac{\sigma_{R-EG}}{\sigma_{I-EG}}}, \quad N'_{EG} = \frac{1}{N_{EG}}. \quad (6)$$

Based on the acoustic impedance, the transmission pulse (σ_{T-EG}) in the front end and the incident pulse (σ'_{I-EG}) in the back end are calculated from

$$\sigma_{T-EG} = \frac{2}{1 + N_{EG}} \sigma_{I-EG}, \quad \sigma'_{I-EG} = \frac{1 + N'_{EG}}{2} \sigma'_{T-EG}. \quad (7)$$

Because the shapes of these stress pulses are approximately same (see Fig. 2(b)), we use the peak values of the stress pulses to simplify the analytical process. The symbols of the peak values are changed by adding the subscript ‘‘P.’’ For example, the symbol of the peak incident pulse in front end becomes σ_{IP-EG} . Figure 2(c) shows the transmission pulse in back end under four different kinds of the incident pulse. The increase of the transmission pulse in back end is accompanied by the incident pulse. According to Eqs. (5) and (7), the theoretical predictions $\bar{\sigma}'_{IP-EG}$ ($z=L_{EG}=94.5$ mm) and the experimental values σ'_{IP-EG} of the peak incident pulse in back end are obtained; see Fig. 3(a) and Table I. The experimental results concerning the peak incident pulse in back end are very close to the theoretical results. Thus, it is found that the pulse energy of the ethylene glycol is dissipated only from the container and it is corroborated that the stress pulses of the ethylene glycol can be used as the reference pulses.

Typical recorded stress pulses of the ethylene glycol and the 62 vol/vol. % dense particle suspension from strain gages attached to the bars are plotted in Fig. 3(b). The incident pulses are nearly identical, indicating that these experiments are performed under the same conditions. A significant difference between the transmission pulse of the ethylene glycol and the suspension is observed apparently. For the transmission pulse of the ethylene glycol, it is found that the pulse is formed with a series of pulses exhibiting an oscillation effect. In the classic SHPB experiment, the oscillation effect of the incident pulse, which is called the geometry

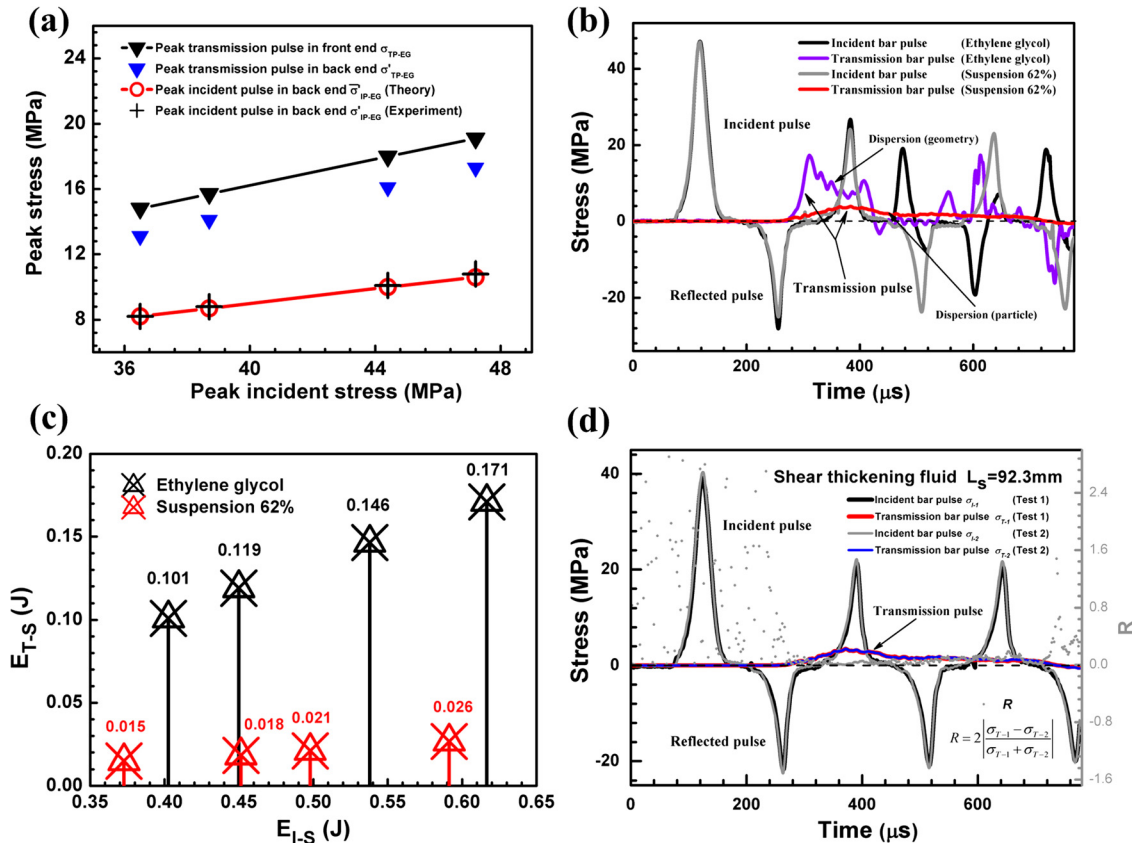


FIG. 3. (a) Peak stress pulse of ethylene glycol on the modified SHPB; (b) Comparison the stress pulses under the peak incident pulse about 47 MPa for the ethylene glycol and the 62 vol/vol. % dense particle suspension; (c) The incident pulse energy (E_{I-S}) and the transmission pulse energy (E_{T-S}) for the ethylene glycol and the suspension; (d) Strain gage signals for two experiments performed under identical impact conditions. The R value is used to verify the contact ratio in two tests. The R value is below 15% in the range of the transmission plus, which indicates the two curves are in good coincidence.

TABLE I. Peak stress pulse of ethylene glycol unit:MPa.

σ_{IP-EG}	σ_{TP-EG}	σ'_{TP-EG}	σ'_{IP-EG}	$\bar{\sigma}'_{IP-EG}$
47.2	19.1	17.3	10.8	10.6
44.4	18.0	16.1	10.1	10.0
38.7	15.7	14.1	8.8	8.7
36.5	14.8	13.1	8.2	8.2

dispersion, can also be found when it does not use the pulse shaper.¹⁵ It can be explained by the Poisson effect, which produces a transverse kinetic energy while the specimen is under axial loading. As previously mentioned, the transverse energy is also found. Thus, the oscillation effect of the transmission pulse of the ethylene glycol is most likely to be caused by the geometry dispersion. However, the first peak is emanated from the incident pulse. Figure 3(b) shows that the transmission pulse of STF compared with the reference pulse has a longer pulse width, and the pulse amplitude is much weaker. It is indicated that the pulse energy loss of the suspension is not just by the container, but by its character.

To make the pulse energy dissipation clear, the incident pulse energy (E_{I-S}) and the transmission pulse energy (E_{T-S}) for the ethylene glycol and the suspension are obtained.

$$\begin{aligned} E_{I-S} &= \frac{c_{AL}A_{AL}}{E_{AL}} \int_0^T \sigma_{I-S}^2(t) dt, \\ E_{T-S} &= \frac{c_{AL}A_{AL}}{E_{AL}} \int_0^T \sigma'_{T-S}^2(t) dt, \end{aligned} \quad (8)$$

where A_{AL} is the cross-sectional area of the Hopkinson bars, the subscript S is the kinds of the specimen. The results are plotted in Fig. 3(c). It can be seen that the transmission pulse energy of the suspension is much smaller than the ethylene glycol, suggesting that the suspension has the ability to absorb the pulse energy, and the transmission pulse energy linearly increases with the incident pulse energy. As mentioned before, the reversibility is important in application. In this letter, two experiments are performed under identical impact conditions and the time between experiments is about 1 min. These results are compared in Fig. 3(d). The incident pulses are nearly identical, indicating that these experiments were performed under the same conditions. The transmission pulses are also near identical, indicating that this behavior for the STF is reversible.

Note that the compression ratio is very important to retain structural integrity under the impact conditions. The displacement in the front end D_F and the displacement in the back end D_B (see Fig. 1) can be obtained as

$$\begin{aligned} D_F &= \frac{c_{AL}}{E_{AL}} \int_0^T [\sigma_{I-S}(t) - \sigma_{R-S}(t)] dt, \\ D_B &= \frac{c_{AL}}{E_{AL}} \int_0^T \sigma'_{T-S}(t) dt. \end{aligned} \quad (9)$$

For the suspension, the compression ratios ($R_{SU} = (D_F - D_B)/L_{SU}$, $L_{SU} = 92.3$ mm) are 0.93‰, 1.04‰, 1.04‰, 1.11‰ for the peak incident stress of 36.5 MPa, 39.1 MPa, 44.4 MPa, and 48.2 MPa, respectively. The value

of the compression ratios is very small; thus the deformation under the impact can be almost neglected.

Theoretical models for describing the energy absorption of the STF are not readily available. However, several arguments put forward by different researchers can be used to understand this phenomenon. The scattering of the stress wave has been confirmed, which is attributed to the inhomogeneous nature of the material. According to the Fourier analysis, the stress wave is composed of a series of simple harmonic wave which has respective frequency and wavelength. The stress dispersion happens in the scattered wave where its wavelength is nearby the dimensions of the scatterer and causes the stress wave attenuation.¹⁶ In this letter, the STF is regarded as a strongly inhomogeneous system, and the silica particles deem as the scatterer. The above mentioned viewpoint is based on the stress dispersion, and the another argument is based on the microstructure of the STF. Recently, Waitukaitis and Jaeger investigated a new mechanism to explain the large impact resistance of the STF.¹⁷ It is found that the particles are forced across the jamming transient and an impact-jammed solid is rapidly growing when a high speed rod direct impact the STF. This jamming solid is transient, but before “melting.” In this letter, when the stress wave transmits through the specimen, the jamming solid could be well formed. During the formation of the jamming solid, the short-range hydrodynamic lubrication force between the particles should be overcome, which further leads to the energy dissipation.¹⁸

In summary, the stress pulse attenuation in STF was investigated by a modified split Hopkinson pressure bar. Because a part of the energy was lost from the container, the neat ethylene glycol was used as the reference. In comparison to the ethylene glycol solution, the transmission pulse amplitude of STF was much weaker and the pulse width is much longer. The transmission pulse energy of STF is much smaller than the ethylene glycol solution. It could be considered that energy dissipation occurred in STF. The compression ratios of STFs under impact loading are below 1.2‰, thus the deformation could be neglected. Finally, different from the traditional energy absorption materials, the energy dissipation behaviour of the STF was reversible.

Financial supports from the National Natural Science Foundation of China (Grant No. 11125210) and the National Basic Research Program of China (973 Program, Grant No. 2012CB937500) are gratefully acknowledged. The authors also thank Professor Shisheng Hu of USTC and his students for their help on the experiment and useful discussions on the results.

¹J. Banhart, *Prog. Mater. Sci.* **46**, 559 (2001).

²D. Karagiozova, G. S. Langdon, and G. N. Nurick, *Int. J. Solids Struct.* **49**, 2763 (2012).

³S. Luding, *Nature* **435**, 159 (2005).

⁴C. Daraio, V. F. Nesterenko, E. B. Herbold, and S. Jin, *Phys. Rev. Lett.* **96**, 058002 (2006).

⁵H. A. Barnes, *J. Rheol.* **33**, 329 (1989).

⁶X. Cheng, J. H. McCoy, J. N. Israelachvili, and I. Cohen, *Science* **333**, 1276 (2011).

⁷X. Z. Zhang, W. H. Li, and X. L. Gong, *Smart Mater. Struct.* **17**, 035027 (2008).

- ⁸Y. S. Lee, E. D. Wetzel, and N. J. Wagner, *J. Mater. Sci.* **38**, 2825 (2003).
- ⁹X. L. Gong, Y. L. Xu, W. Zhu, S. H. Xuan, W. F. Jiang, and W. Q. Jiang, "Study of the knife stab and puncture-resistant performance for shear thickening fluid enhanced fabric," *J. Compos Mater.* (published online).
- ¹⁰X. Z. Zhang, W. H. Li, and X. L. Gong, *Smart Mater. Struct.* **19**, 125012 (2010).
- ¹¹Y. Tian, J. L. Jiang, Y. G. Meng, and S. Z. Wen, *Appl. Phys. Lett.* **97**, 151904 (2010).
- ¹²R. L. David, *CRC Handbook of Chemistry and Physics*, 90th ed. (CRC, Boca Raton, 2010), p. 2320.
- ¹³F. B. Surani, X. G. Kong, D. B. Panchal, and Y. Qiao, *Appl. Phys. Lett.* **87**, 163111 (2005).
- ¹⁴E. V. Lomakin, P. A. Mossakovsky, A. M. Bragov, A. K. Lomunov, A. Y. Konstantinov, M. E. Kolotnikov, F. K. Antonov, and M. S. Vakshtein, *Arch. Appl. Mech.* **81**, 2007 (2011).
- ¹⁵D. J. Frew, M. J. Forrestal, and W. Chen, *Exp. Mech.* **42**, 93 (2002).
- ¹⁶G. Mavko, T. Mukerji, and J. Dvorkin, *The Rock Physics Handbook: Tools for Seismic Analysis of Porous Media* (Cambridge University, New York, 1998), p. 124.
- ¹⁷S. R. Waitukaitis and H. M. Jaeger, *Nature* **487**, 205 (2012).
- ¹⁸J. F. Brady and G. Bossis, *Annu. Rev. Fluid Mech.* **20**, 111 (1988).